ELSEVIER

Journal of Chromatography A, 915 (2001) 43–52

JOURNAL OF CHROMATOGRAPHY A

www.elsevier.com/locate/chroma

Peak purity assessment in liquid chromatography–mass spectrometry

Dan Bylund, Rolf Danielsson, Karin E. Markides*

Department of Analytical Chemistry, Uppsala University, P.O. Box 531, 751 21 Uppsala, Sweden

Received 2 October 2000; received in revised form 12 December 2000; accepted 3 January 2001

Abstract

Fixed-size moving window evolving factor analysis and base peak chromatograms have been used for peak purity detection in data generated with LC–MS. The two methods were evaluated with both real and simulated data and were found to be fast and complementary to each other. When a possibly impure peak is detected, it is suggested that further information can be obtained from local principal component analysis modelling and comparative mass chromatogram plots.

Keywords: Peak purity detection; Principal component analysis; Fixed-size moving window; Evolving factor analysis

1. Introduction

After the introduction of interfaces based on atmospheric pressure ionisation there has been a breakthrough for mass spectrometry (MS) as a detection method for liquid chromatography (LC). Using LC–MS, the characterisation of the sample can be based on mass spectral information as well as retention times, which gives a unique selectivity in the analysis of complex samples. The second dimension in the generated data also gives the opportunity to apply multivariate analysis in the interpretation of results.

One of the important areas for the application of chemometrics to hyphenated chromatography and detection data is the determination of peak purity. During the last decades, a large number of techniques for the assessment of the peak purity in this kind of bilinear data have been established [1–6]. Most of them were developed for data generated with liquid chromatography and diode array detection (LC–DAD). Some studies have also been reported where available methods have been compared in their performance with LC–DAD data [7–9]. However, only a few reports have been published describing the possibility to apply these techniques to LC–MS data [10,11] or gas chromatography (GC)–MS data [12]. In contrast to most other spectroscopic data, mass spectral data are discrete in nature, i.e., the analyte responses are present for a few ions rather than as a continuous spectrum. Differences can also be seen in the noise structure with, e.g., spurious spikes. There is also a higher extent of signal dependent noise due to the counting principle.

The main goal of this study was to suggest a strategy for producing a quick overview of the peak purity in large LC–MS data sets. The chemometric techniques applied for peak purity analysis were

*Corresponding author. Tel.: +46-18-4713-691; fax: +46-18-4713-692.

E-mail address: karin.markides@kemi.uu.se (K.E. Markides).

0021-9673/01/$ – see front matter
PII: S0021-9673(01)00543-X

principal component analysis (PCA) [13] and fixed-size moving window evolving factor analysis (FSMW-EFA) [2]. The methods were used on both simulated and experimentally obtained LC–MS data. With simulated data the possibility of detecting an impurity with FSMW-EFA was quantified and the dependence on impurity characteristics was systematically investigated. The results were compared with the base peak chromatogram (BPC), a visual technique implemented in commercial software [14]. These techniques for impurity detection were also compared for real LC–MS data.

When a possibly impure peak is detected, there is a need for a more thorough examination. With local PCA modelling, the ions of interest may be identified and the corresponding chromatographic profiles can be compared visually. The benefits of this procedure were demonstrated for real LC–MS data in comparison with more conventional ways of data presentation (total ion and extracted ion chromatograms, mass spectrum at peak maximum or summed over peak duration).

Peak purity profiling is a first step in order to establish the pure spectra and concentrations of the solutes. Further data analysis may involve curve resolution [15–17] or methods that rely on peak profiles [18,19]. The peak purity detection strategy described in this work makes it possible to focus further efforts on a minor set of possible peak clusters. Hence it can be considered as a pre-processing step prior to more elaborate, often computer intensive, methods.

2. Theory

2.1. LC–MS data

The data from a scanning LC–MS experiment can be organised as an $M \times N$ data matrix (**D**), with M rows of mass spectra and N columns of mass chromatograms. Contributors to **D** are analyte signals (**A**), background (**B**) and noise (**E**) according to:

$$\mathbf{D} = \mathbf{A} + \mathbf{B} + \mathbf{E} \tag{1}$$

The bilinear matrix **A** can be further separated into the individual mass spectra (**s**) and concentration profiles (**c**) for K analytes, which leads to:

$$\mathbf{D} = \sum_{k=1}^{K} \mathbf{c}_k \mathbf{s}^{\mathrm{T}}{}_k + \mathbf{B} + \mathbf{E} = \mathbf{C}\mathbf{S}^{\mathrm{T}} + \mathbf{B} + \mathbf{E} \tag{2}$$

where the superscript T indicates the transpose.

An important difference for LC–MS, as compared to LC–DAD data, is the more discrete nature of the spectral matrix **S**. This could be advantageous since it is easier to achieve spectral selectivity, but it also means that a lot of channels only carry background and noise, which may effect the multivariate data analysis negatively. With only few correlated variables the analyte related contribution $\mathbf{C}\mathbf{S}^{\mathrm{T}}$ to the data matrix **D** is less prominent, hence the PCA modelling is less effective in discriminating useful information from background and noise.

2.2. Fixed-size moving window evolving factor analysis

Evolving factor analysis methods [20] are based on PCA. With PCA an $I \times J$ data matrix **X** is decomposed into F significant latent variables according to:

$$\mathbf{X} = \mathbf{T}\mathbf{P}^{\mathrm{T}} + \mathbf{R} \tag{3}$$

Here **T** is the $I \times F$ score matrix, **P** is the $J \times F$ loading matrix, and **R** is the $I \times J$ residual matrix. The value of F, the so-called pseudorank, indicates the chemical rank of the system, and can be determined by error analysis [21]. The eigenvalues (λ) associated with the principal components can be calculated as the inner product of the score vectors:

$$\lambda_{\mathrm{f}} = t_{\mathrm{f}}^{\mathrm{T}} t_{\mathrm{f}} \tag{4}$$

In its original form, EFA is performed by applying PCA on a window of increasing size and monitoring the eigenvalues [1]. Keller and Massart refined the method to work with a window of constant size moving through the data matrix [2]. In FSMW-EFA a change in the chemical rank of the system is indicated by peakshaped changes in the monitored eigenvalues. Thereby impurities will show up as peaks in the second and higher eigenvalue plots.

Since the eigenvalues may differ in many orders

of magnitudes, visual interpretation is often aided by monitoring their logarithms or the singular values instead. The singular values (θ), defined as the positive square roots of the corresponding eigenvalues, have been used throughout this work.

The idea of FSMW-EFA is that the matrix product $\mathbf{CS}^T$ in Eq. (2) corresponds to $\mathbf{TP}^T$ in Eq. (3).

The possibility of detecting an impurity with FSMW-EFA is mainly dependent on the degree of spectral similarity (cf. **S**) the chromatographic resolution (cf. **C**), and the signal intensities. A comparison of Eqs. (2) and (3) reveals that the presence of background (**B**) and noise (**E**) must be considered. Different non-ideal properties in the data can generate ''false'' changes in the secondary eigenvalues. Such artefacts may disturb the evaluation, either by being misinterpreted as a real change in the chemical rank or by masking the effects of a real impurity. Unless high level background is subtracted, peaks in the second eigenvalue will appear in the vicinity of the inflection points of the pure peak (Fig. 1). Similar effects can be introduced by deviations from bilinearity, e.g., caused by non-linear detector response. Signal dependent noise is also a problem with FSMW-EFA. If the noise increases with the signal, all of the secondary eigenvalues will increase at the peak maximum. Proper scaling of the data can partly solve this problem [22].

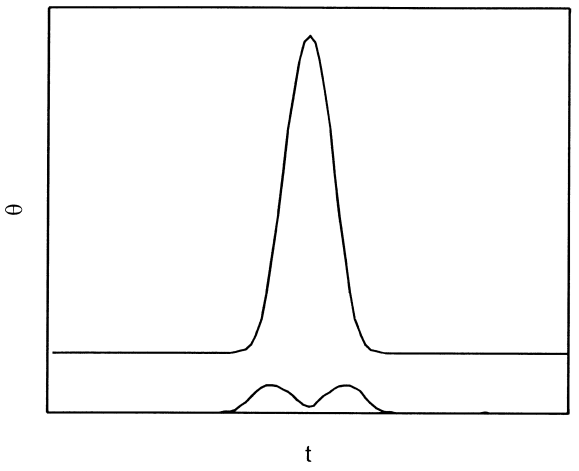

Fig. 1. FSMW-EFA plot (θ vs. t) for a Gaussian LC–MS peak with constant non-zero background. The background causes an elevated baseline level in the first singular value ($\theta 1$) and two peaks in $\theta 2$. The latter may be misinterpreted as an indication of impurities.

2.3. Base peak chromatogram

In a BPC, the highest intensity in each spectral scan is plotted versus time. The method is suitable to locate and identify small peaks as long as the strongest analyte signal is significantly above the highest background signal. When a BPC is used for peak purity analysis, the identity of the ion giving the highest signal must be indicated. With the Multiview software (v.1.3; PE Sciex, Concord, Canada), this is established by a plot colour change when the ion identity changes significantly. Thus an impure peak is indicated by a colour change within the peak. For this procedure to work, the impurity base peak mass must differ from that of the main compound, and also be of higher intensity for some position within the peak cluster.

2.4. Comparative mass chromatogram plot

A plot of a mass chromatogram versus another mass chromatogram from the same experiment, here referred to as a comparative mass chromatogram plot (CMCP), can reveal interesting information. If the two masses are present in the same peak, three major features can be identified. Identical retention time and peak shape result in a straight line with the slope determined by the peak height ratio (Fig. 2a). A bow shape reveals a difference in peak width or the presence of non-linearity (Fig. 2b). A difference in retention time, finally, gives a loop, where the direction is determined by the retention order (clockwise when the y-mass elutes before the x-mass) (Fig. 2c). The major problem with CMCP is that it is not always possible to identify the masses of interest. A working strategy may be to utilise loading plots from local PCA models [23] for this purpose. It should also be mentioned that narrow loops in a CMCP might be an artefact introduced by the scan time. This problem can be circumvented by data preprocessing, e.g., through the method described by Pool et al. [24].

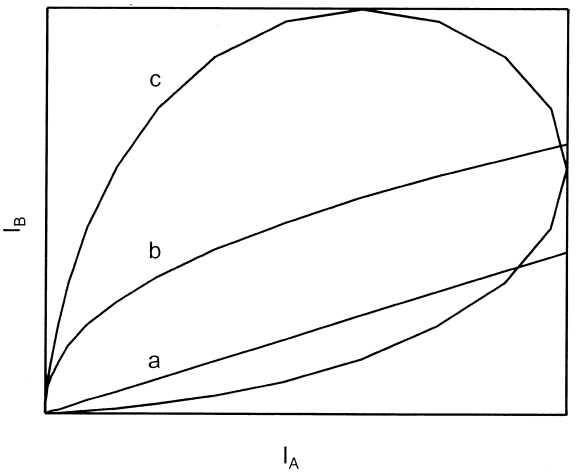

Fig. 2. CMCP plots (I_B vs. I_A) for three typical cases: (a) identical retention and peak shape represented by a straight line; (b) a difference in peak width represented by a bow shape; (c) a retention time shift represented by a loop pattern.

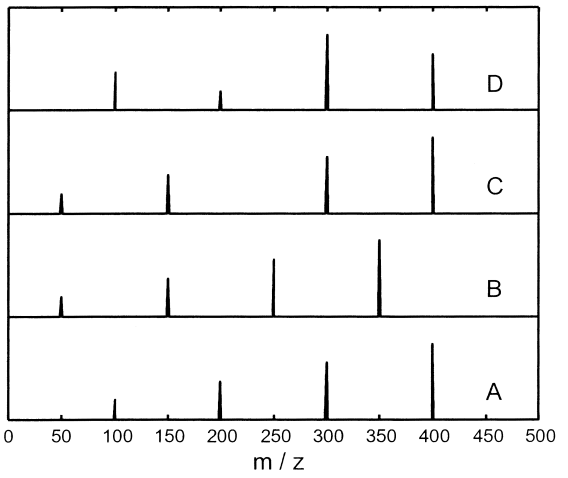

Fig. 3. Simulated mass spectra for three impurities (B–D) with varying degree of spectral similarity compared to the main compound (A).

3. Experimental

3.1. Real LC–MS data

An extract of rosemary was prepared by placing a suspension of 300 mg dried, ground rosemary in 7 ml 10 m*M* acetic acid in an ultrasonic bath for 90 min. After filtration, 20 μl of the extract was injected into an isocratic (10 m*M* acetic acid–methanol, 7:3) LC–MS system consisting of an LKB 2150 pump (Bromma, Sweden) run at 0.4 ml/min, a Genesis C_{18} column (150×3 mm, 4 μm) from Jones Chromatography (Hengoed, UK), and an API 365 mass spectrometer (PE Sciex, Concord, Canada). Before electrospray ionisation, the flow was split to give approximately 20 μl/min to the MS system operated in the positive Q1 scan mode.

3.2. Simulations

Fig. 3 shows the simulated mass spectra of compounds A–D. These spectra were constructed to give different degrees of spectral similarity between the main compound A and the impurities B–D, thereby illustrating different challenges in peak purity analysis of LC–MS data. As a measure of the similarity of two spectra, the angle β between the two corresponding data vectors **X** and **Y** may be taken (see Eq. (5)):

$$\cos\beta = \frac{\sum_i x_i y_i}{\sqrt{\sum_i x_i^2 \sum_i y_i^2}} \quad (5)$$

The spectrum of impurity B is completely different from that of the main compound ($\beta = 90°$), while spectrum C has some ions in common with A and some unique ions ($\beta = 30°$). The impurity C illustrates a situation that could arise from isobaric compounds or compounds with isobaric building blocks. Spectrum D differs from A only in the relative intensity of the ions ($\beta = 20°$), illustrating the analysis of structural isomers. The chromatographic profiles were generated as pure Gaussian peaks for the main compound and one of the impurities. Finally random numbers, representing white noise, were added to the data matrix.

The noise level (σ_{noise}), the relative amount of impurity (%I) and the chromatographic resolution (R_s) of the two peaks were varied according to a full factorial design (Table 1). The design was replicated four times in order to evaluate the random variations.

A second series of simulations was intended for a closer examination of the effect of the resolution on FSMW-EFA. Here the resolution was increased in

Table 1
Factorial design settings for the study on simulated data

Run	R_s	σ_{noise}	%I
1	0.25	5	5
2	0.50	5	5
3	0.25	10	5
4	0.50	10	5
5	0.25	5	10
6	0.50	5	10
7	0.25	10	10
8	0.50	10	10

small steps for two levels of the relative amount of the impurity. These data were simulated without noise.

3.3. Data analysis

All calculations were performed with MATLAB (v.4.2c; MathWorks, Natick, MA, USA) run on a personal computer with a Pentium II 400 MHz processor and 128 MB RAM. The MATLAB codes for FSMW-EFA and BPC were written in the laboratory, while the Chemometrics Toolbox (MathWorks) was used for PCA. The FSMW-EFA analyses were performed with a constant window size of seven data points.

For the real data, possibly impure peaks were identified by visual inspection of the FSMW-EFA plot. For these peaks comparisons were made between FSMW-EFA plots and BPCs, between ordinary mass spectra and PCA loading plots, and between extracted ion chromatograms and CMCPs.

For the simulated data, the detectability of impurities with FSMW-EFA was quantified by the signal-to-noise ratio for the second singular value as:

$$S/N = \frac{\theta 2_{peak} - \theta 2_{bg}}{s_{\theta 2,bg}} \quad (6)$$

where $\theta 2_{peak}$ and $\theta 2_{bg}$ is the maximum and the background levels, respectively, of the second singular value and $s_{\theta 2,bg}$ is the estimated standard deviation of the background fluctuations. The results were compared with those from BPC, for which the impurity was defined as detected when the base peak mass switched within the apparent single peak.

4. Results and discussion

4.1. Real LC–MS data

The total ion chromatogram for the rosemary data (Fig. 4) showed a large number of peaks emerging from flavonoids and diphenolic substances [25,26]. FSMW-EFA on this data set took less than a second to perform, and a number of possibly impure peaks were identified in the eigenvalue plot. The evaluation of the peaks 1–3 in Fig. 4 will be discussed here.

For the first possible peak cluster (1) the signal-to-noise and signal-to-background ratios were high, and no pre-treatment of the data was necessary for impurity detection with FSMW-EFA (Fig. 5a) or BPC (Fig. 5b). The summed mass spectrum over the peak showed a number of significant ions (Fig. 6a), and the extracted ion chromatograms (XICs) of the two most intense ions clearly revealed a retention time difference (Fig. 6b). Alternatively, the ions of interest could be identified in the loading plot for a local PCA model (Fig. 6c), and the retention time difference revealed by the loop pattern of the CMCP (Fig. 6d). The two peaks were found to be of equal size with chromatographic resolution $R_s = 0.40$.

The low signal-to-background ratio for the second possible peak cluster (2) made the FSMW-EFA plot hard to interpret (Fig. 7a) and the BPC less informative (Fig. 7c). However, after background subtraction

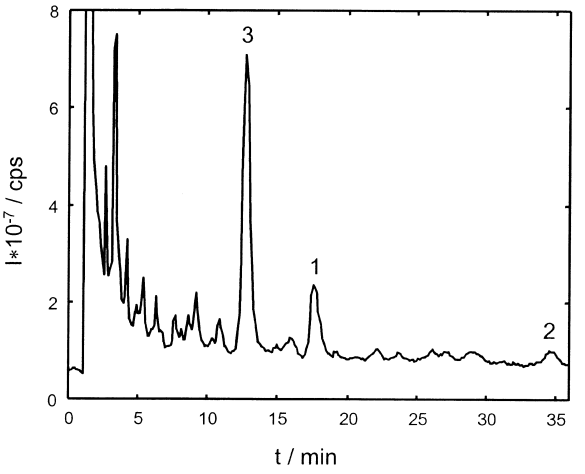

Fig. 4. The total ion chromatogram for an LC–MS analysis of a rosemary extract. Three possibly impure peaks are labelled.

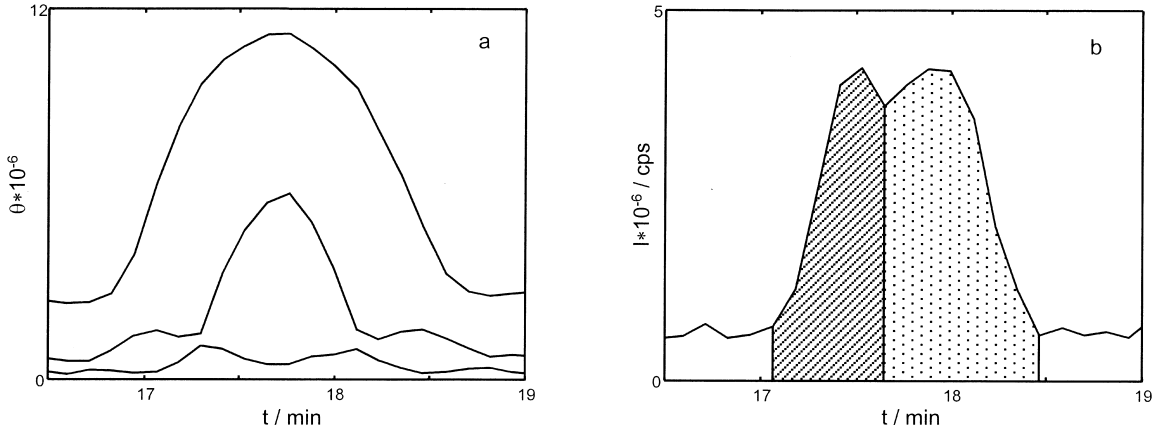

Fig. 5. Peak purity profiling of peak 1: (a) the FSMW-EFA plot shows a large peak in $\theta 2$ that is not present in $\theta 3$, thereby strongly suggesting that the peak is impure; (b) the BPC shows that the base peak mass switches within the peak.

[27] both methods succeeded in classifying the peak as impure (Fig. 7b and d). A number of significant ions were observed in the summed mass spectrum of the peak (Fig. 8a). However, from the completely overlapping peaks in the XIC (not shown) it was deduced that the two most intense ions emerged from the same compound. Here the loading plot from a local PCA model (Fig. 8b) is more informative since it gives different directions for ions related to different compounds. Both the XICs and the CMCP of the two most important ions in the loading plot (m/z 285 and m/z 347) clearly showed a retention time difference, and the cluster was found to contain two peaks with area ratio 1:3 and resolution $R_s = 0.53$.

No indication of impurity was found in the BPC for the last possible peak cluster (3), neither before nor after background subtraction. The FSMW-EFA plot, however, did show an increase in the second singular value but also in the third singular value (Fig. 9a), which indicates the presence of signal-dependent noise. The mass spectrum of the peak showed a number of significant ions (Fig. 9b). More information about these ions was obtained from the PCA loading plot (Fig. 9c), where the main ion was identified as m/z 331. The isotope ion m/z 332 was somewhat displaced from the direction of the main ion, which indicates the presence of non-linear detector response. The ion m/z 661, with considerable loadings in a different direction, was suspected as an impurity. However, the CMCP for m/z 661 versus m/z 331 (Fig. 9d) showed the typical bow shape pattern for non-linearity. It could be concluded that m/z 331 was the protonated molecule ion $[M+H]^+$ and m/z 661 its dimer $[2M+H]^+$.

The evaluation of the peak cluster (3) shows a number of possible explanations for an increase of the second singular value, not caused by an impurity. Firstly, the size of the peak led to saturation in the detector for the most abundant ion. Secondly, the large spread in responses led to a manifest effect of the signal-dependent noise level in mass spectrometric data. Finally, the concentration dependence in the formation of dimers [28] acted as a second source of non-linearity.

4.2. Simulations

The results for the ideal and controlled situations with simulated data from Table 1 are summarised in Table 2. The detectability with FSMW-EFA according to Eq. (6) was obtained as the mean S/N for the replicate runs. As one might have expected the detectability increased with higher resolution and higher impurity levels, and decreased with higher noise levels and higher degree of spectral similarity. With analysis of variance (ANOVA), significant interactions between the quantitative factors were also found, although the controlled variation of noise level makes the concept of statistical significance less clear.

From theory it is known that the standard devia-

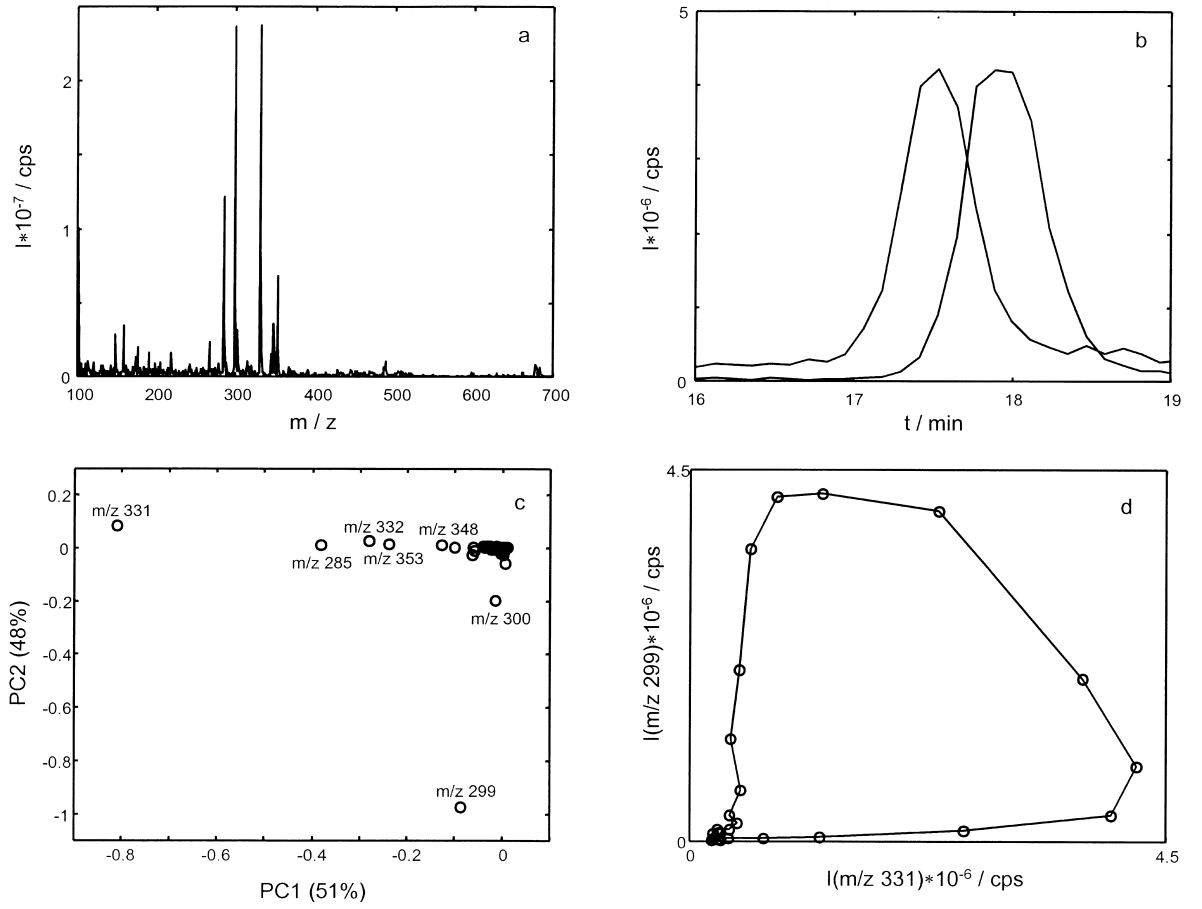

Fig. 6. Further evaluation of peak 1: (a) the mass spectrum of the peak; (b) the XICs for m/z 299 and m/z 331 clearly show a retention time difference; (c) the loading plot for a mean-centred PCA model shows two major directions, one headed by m/z 331 and one headed by m/z 299; (d) the CMCP for m/z 299 versus m/z 331 shows the typical pattern of a retention time difference (cf. Fig. 2).

tion for any singular value (σ_θ) equals the standard deviation of the measurement error [29]. Therefore, doubling the noise level according to the design doubles $\sigma_{\theta 2,\mathrm{bg}}$ as well as the background level $\theta 2_{\mathrm{bg}}$. Hence the nominator in Eq. (6) is somewhat reduced while the denominator is doubled. As a result the FSMW-EFA detectability is more than halved with a doubling of the noise level.

A change in the relative amount of impurity has an impact on the $\theta 2_{\mathrm{peak}}$ but does not change $\theta 2_{\mathrm{bg}}$ or $\sigma_{\theta 2,\mathrm{bg}}$. The results indicate that doubling the impurity level more than doubles the detectability. The actual effect depends on the value of $\theta 2_{\mathrm{bg}}$, i.e., there is an interaction between the impurity level and the noise level.

When comparing the FSMW-EFA results for the different impurities (Table 2), almost linear relations were found. This implies that the effects of impurity level, chromatographic resolution, and noise level are quite similar for the different kinds of impurity spectra: $S/N = \mathrm{constant} \cdot f$ (%I, R_s, σ_{noise}). The constant decreases with the similarity between the impurity and the main compound. With unity value for compound B, the constant was found to be 0.43 and 0.26 for compounds C and D.

The resolution has a non-linear effect on peak height of the second singular value as found from the separate data set. At very low resolution the concentration profile of the impurity strongly overlaps that of the main compound, and both are well

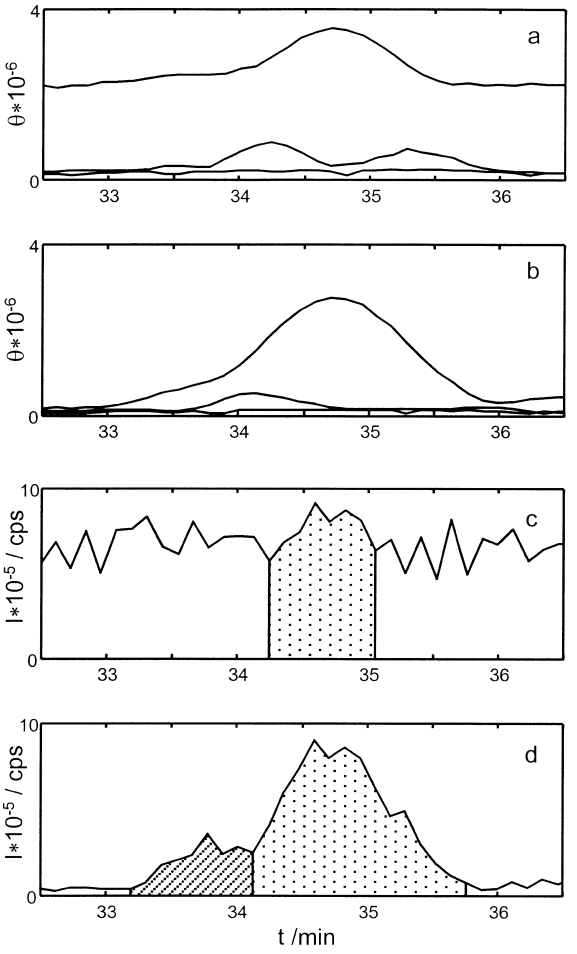

Fig. 7. FSMW-EFA and BPC plots for peak 2: (a) for the raw data a single peak is found in $\theta 1$ and two peaks in $\theta 2$, which is expected for a pure peak on non-zero background (cf. Fig. 1); (b) after background subtraction $\theta 1$ is no longer unimodal and $\theta 2$ shows a single maximum indicating the presence of two analytes within the peak cluster; (c) for the raw data no peak at all seems to be present. However, a segment with m/z 347, differing from the surrounding dominating background ion, is found. (d) After background subtraction an asymmetric peak with two distinct ion segments (m/z 285 and 347) can be distinguished.

described by the first principal component. As a result the second singular value remains low. As the resolution increases the degree of overlap decreases, more of the variance is described by the second principal component, and the peak in $\theta 2$ grows. This increase with resolution continues until the impurity is visible already in $\theta 1$. Further increase in resolution actually means that the peak maximum in $\theta 2$ declines. However, this does not mean a lower detectability since peak purity with FSMW-EFA is assessed from the overall picture. At still higher resolution, the FSMW-EFA plot of the first singular value will not be unimodal and the impurity can be observed directly as an extra peak in that profile [30].

The possibility of detecting impurities by BPCs was also investigated. As a measure of detectability, the numbers of cases of positive detection for the four replicates are reported in Table 2. The results for compounds B and D indicate that the resolution has a major impact on the detectability with BPC. For compound D, of which the spectrum was most similar to that of the main compound, BPC was found to be a useful complement to FSMW-EFA. This is explained by the fact that BPC, contrary to FSMW-EFA, is insensitive to spectral similarity as long as the base peak mass differs. Since the base peak mass was the same for compounds A and C, BPCs could not be successful in those cases.

5. Conclusions

In order to examine the peak purity in complex LC–MS data, FSMW-EFA plots and BPCs are fast and complementary tools. When possible impure peaks or clusters are detected, local PCA models and CMCPs in combination with chemical knowledge give further information. The special properties of data generated with mass selective detection, in comparison with diode array detection, should be considered. Although it may be easier to find fully selective signals, the influence of background and noise is more pronounced. Hence application of preprocessing methods for background suppression and noise reduction should be included in the peak purity detection strategy.

Acknowledgements

Financial support from the Swedish Natural Research Council project K-1439-326 and from the Swedish Foundation for Strategic Research is gratefully acknowledged.

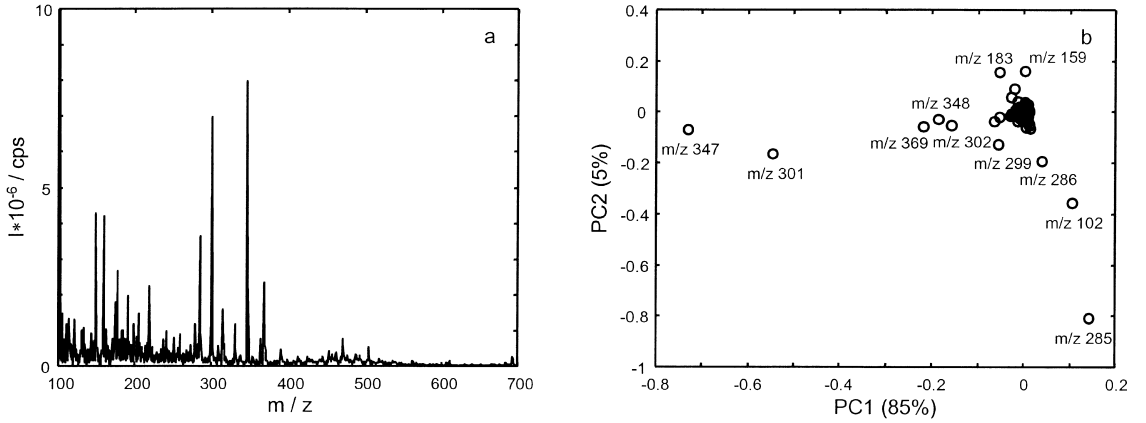

Fig. 8. Further evaluation of peak 2: (a) the mass spectrum of the peak; (b) the loading plot for a mean-centred PCA model shows two major directions, one headed by m/z 347 and one headed by m/z 285.

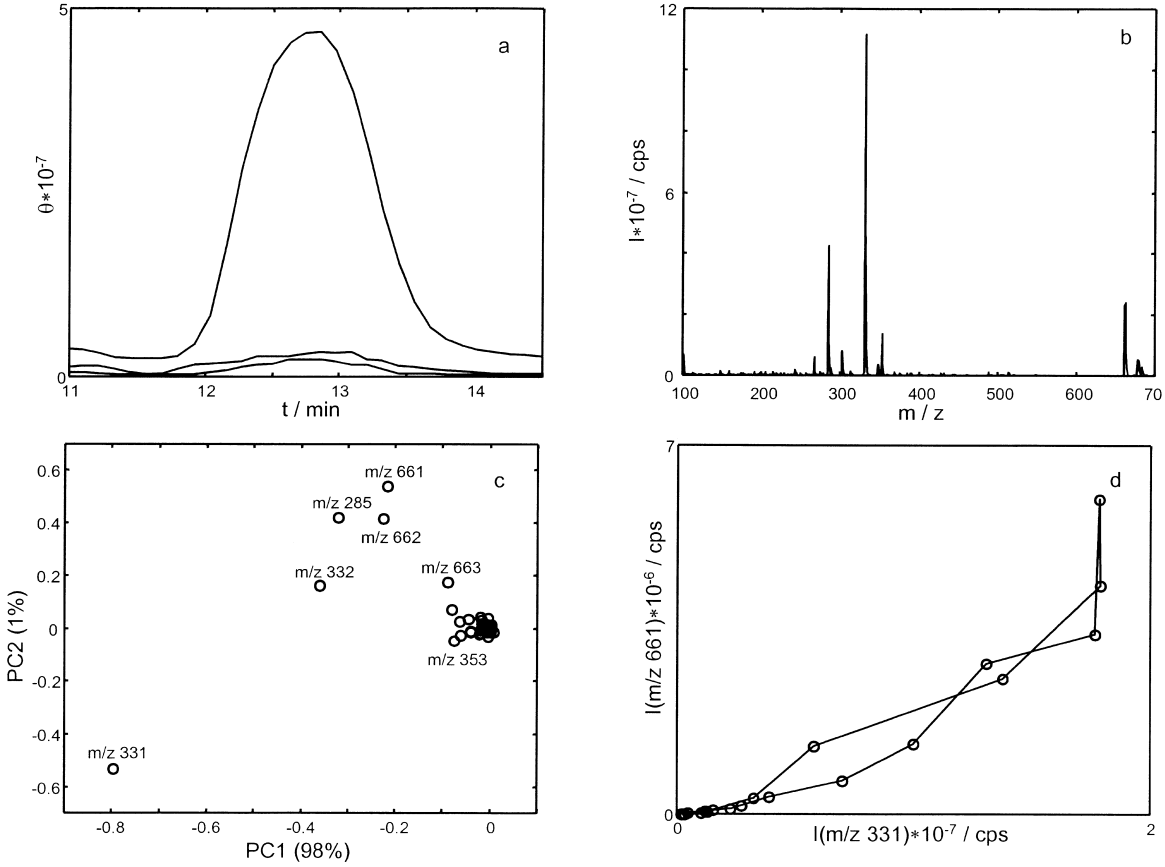

Fig. 9. Peak purity profiling of peak 3: (a) the FSMW-EFA plot shows an increase in $\theta 2$ within the $\theta 1$ peak, which indicates the presence of an impurity. The pattern for $\theta 3$, however, is similar to that of $\theta 2$, and the maximum is close to the maximum of $\theta 1$. Therefore, the peak is most likely pure, and the increase of $\theta 2$ and $\theta 3$ is due to signal-dependent noise; (b) the mass spectrum of the peak; (c) the loading plot for a mean-centred PCA model reveals the ions of interest but shows no clear relationships between them; (d) the CMCP for m/z 661 versus m/z 331 shows a bow shape, typical for a peak width deviation (cf. Fig. 2).

Table 2
FSMW-EFA and BPC results for the different impurities (B–D)[a]

Run	A+B		A+C		A+D	
	FSMW-EFA[b]	BPC[c]	FSMW-EFA[b]	BPC[c]	FSMW-EFA[b]	BPC[c]
1	46.7	0	19.9	0	11.3	0
2	77.7	4	37.2	0	17.9	4
3	16.8	0	6.8	0	3.8	0
4	33.6	4	14.6	0	7.1	4
5	90.8	0	44.6	0	24.8	1
6	173.7	4	72.5	0	46.8	4
7	43.4	0	17.1	0	9.9	0
8	79.2	4	32.3	0	18.1	4

[a] Experimental settings from Table 1.
[b] Average S/N in the second singular value, $n=4$.
[c] Number of impurity detections, $n=4$.

References

[1] M. Maeder, Anal. Chem. 59 (1987) 527.
[2] H.R. Keller, D.L. Massart, Anal. Chim. Acta 246 (1991) 379.
[3] T.D. Jarvis, J.H. Kalivas, Anal. Chim. Acta 266 (1992) 13.
[4] O.M. Kvalheim, Y. Liang, Anal. Chem. 64 (1992) 936.
[5] B.G.M. Vandeginste, W. Derks, G. Kateman, Anal. Chim. Acta 173 (1985) 253.
[6] F. Cuesta Sánchez, M.S. Khots, D.L. Massart, J.O. De Beer, Anal. Chim. Acta 285 (1994) 181.
[7] F. Cuesta Sánchez, B. van den Bogaert, S.C. Rutan, D.L. Massart, Chemometr. Intell. Lab. Syst. 34 (1996) 139.
[8] F. Cuesta Sánchez, S.C. Rutan, M.D. Gil García, D.L. Massart, Chemometr. Intell. Lab. Syst. 36 (1997) 153.
[9] S. Dunkerley, R.G. Brereton, J. Crosby, Chemometr. Intell. Lab. Syst. 48 (1999) 99.
[10] D. Lincoln, A.F. Fell, N.H. Andersson, D. England, J. Pharm. Biomed. 10 (1992) 837.
[11] J.S. Salau, M. Honing, R. Tauler, D. Barceló, J. Chromatogr. A 795 (1998) 3.
[12] L. Roach, M. Guilhaus, Org. Mass Spectrom. 27 (1992) 1071.
[13] S. Wold, K. Esbensen, P. Geladi, Chemometr. Intell. Lab. Syst. 2 (1987) 37.
[14] MultiView User's Manual, PE Sciex, 1996.
[15] A. Garrido Frenich, M. Martínez Galera, J.L. Martínez Vidal, D.L. Massart, J.R. Torres-Lapasió, K. De Braekeleer, J.-H. Wang, P.K. Hopke, Anal. Chim. Acta 411 (2000) 145.
[16] E.J. Karjalainen, U.P. Karjalainen, Anal. Chim. Acta 250 (1991) 169.
[17] K. De Braekeleer, A. de Juan, D.L. Massart, J. Chromatogr. A 832 (1999) 67.
[18] J.E. Biller, K. Biemann, Anal. Lett. 7 (1974) 515.
[19] S.E. Stein, J. Am. Soc. Mass Spectrom. 10 (1999) 770.
[20] J. Toft, Chemometr. Intell. Lab. Syst. 29 (1995) 189.
[21] K. Faber, B.R. Kowalski, Anal. Chim. Acta 337 (1997) 57.
[22] C. Ritter, J.A. Gilliard, J. Cumps, B. Tilquin, Anal. Chim. Acta 318 (1995) 125.
[23] K.D. Zissis, S. Dunkerley, R.G. Brereton, Analyst 124 (1999) 971.
[24] W.G. Pool, J.W. de Leeuw, B. van de Graaf, J. Mass Spectrom. 31 (1996) 213.
[25] T. Staaf, C.F. Bökman, D. Bylund, unpublished results.
[26] M.N. Maillard, P. Giampaoli, Talanta 43 (1996) 339.
[27] D. Bylund, R. Danielsson, G. Malmquist, K.E. Markides, poster presented at the 14th International Mass Spectrometry Conference, Tampere, 1997.
[28] M. Stefansson, P.J.R. Sjöberg, K.E. Markides, Anal. Chem. 68 (1996) 1792.
[29] N.M. Faber, M.J. Meinders, P. Geladi, M. Sjöström, L.M.C. Buydens, G. Kateman, Anal. Chim. Acta 304 (1995) 257.
[30] F. Cuesta Sánchez, J. Toft, O.M. Kvalheim, D.L. Massart, Anal. Chim. Acta 314 (1995) 131.